Inorganic Chemistry

Article

pubs.acs.org/IC

A Series of [Co(Mabiq)Cl_{2-n}] (n = 0, 1, 2) Compounds and Evidence for the Elusive Bimetallic Form

Emma V. Puttock,[†] Priyabrata Banerjee,[‡,§] Manuel Kaspar,[⊥] Liam Drennen,[†] Dmitry S. Yufit,[†] Eckhard Bill,[‡] Stephen Sproules,[∥] and Corinna R. Hess*[,⊥]

[⊥]Department of Chemistry and Catalysis Research Center, Technische Universität München (TUM), Lichtenbergstrasse 4, D-85747 Garching, Germany

[†]Department of Chemistry, Durham University, South Road, Durham, DH1 3LE, United Kingdom

[‡]Max-Planck-Institut für Chemische Energiekonversion, Stiftstrasse 34−36, D-45470 Mülheim an der Ruhr, Germany

[∥]WestCHEM, School of Chemistry, University of Glasgow, Glasgow, G12 8QQ, United Kingdom

Supporting Information

ABSTRACT: The synthesis and characterization of a series of cobalt compounds, coordinated by the redox-active macrocyclic biquinazoline ligand, Mabiq [2−4:6−8-bis(3,3,4,4-tetramethyldihydropyrrolo)-10−15-(2,2′-biquinazolino)-[15]-1,3,5,8,10,14-hexaene-1,3,7,9,11,14-N_6], is presented. The series includes the monometallic Co(Mabiq)Cl_2 (**1**), Co(Mabiq)Cl (**2**), and Co(Mabiq) (**4**), with formal metal oxidation states of 3+ → 1+. A binuclear cobaltous compound, Co_2(Mabiq)Cl_3 (**3**), also was obtained, providing the first evidence for the ability of the Mabiq ligand to coordinate two metal ions. The electronic structures of the paramagnetic **2** and **3** were examined by electron paramagnetic resonance spectroscopy and magnetic susceptibility studies. The Co^{II} ion that resides in the N_4-macrocylic cavity of **2** and **3** adopts a low-spin $S = {}^1/_2$ configuration. The bypirimidine functionality in **3** additionally coordinates a high-spin $S = {}^3/_2$ cobaltous ion in a tetrahedral environment. The two metal ions in **3** are weakly coupled by magnetometry. The square-planar, low-valent **4** offers one of a limited number of examples of structurally characterized N_4-macrocyclic Co^I compounds. Spectroscopic and density functional theory computational data suggest that a Co^{II}(Mabiq$^•$) description may be a reasonable alternative to the Co^I formalism for this compound.

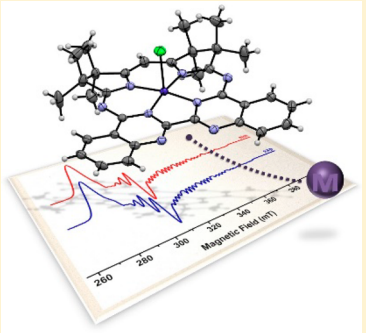

INTRODUCTION

Macrocyclic cobalt complexes have recently become a target of acute focus in the quest for economical and robust solar fuel catalysts.[1−5] Members of this family of compounds, which includes cobalt porphyrins, cobalamins, and cobaloximes, evolve hydrogen electrocatalytically, often operating at modest overpotentials.[6,7] Notably, recent studies have evidenced photocatalytic H_2 production by such systems,[8−11] a vital feature for their integration in an artificial photosystem.[1,12,13]

In-depth mechanistic studies have provided valuable insight into the reactivity of cobalt N_4-macrocyclic complexes and enabled the identification of key reactive intermediates.[1−3,12,14−17] The low-valent Co^I form is commonly the active species in the reaction of the compounds. Protonation of the Co^I species yields a cobalt^{III} hydride, from which H_2 is subsequently released via either a homolytic or heterolytic pathway, restoring the cobaltous form of the complexes. The macrocyclic ligands must, therefore, minimally be able to support metal oxidation states ranging from 1+ to 3+ throughout the catalytic cycle. Cobalt(0) species also have been invoked for H_2 evolution by cobalt porphyrins and cobaloximes with weak acids.[1,5,17]

Given the aforementioned series of electron transfer events, the redox activities of the various N_4-macrocyclic ligands are noteworthy. The pyrrole-based porphyrin and corrole ligands are readily oxidized.[18,19] Indeed, Spiro et al. anticipated that the porphyrin $\pi-\pi^*$ transitions could be exploited for the formation of a Co^I porphyrin radical cation, offering a route to photochemical H_2 production.[18] More recently, partial reduction and protonation of the macrocyclic ligand have been proposed to occur in the mechanism of H_2 evolution by hangman porpyhrins.[20] The diimine moieties of the cobaloximes also are readily reduced.[21,22] Ligand-centered redox processes were established in the chemistry of iron tetraimine complexes,[23] and by analogy, a Co^I cobaloxime ligand radical was proposed as an alternate formulation of the Co^0 species noted above.[1]

Besides their capacity for H_2 production, macrocyclic cobalt complexes have proven to be effective catalysts for a variety of other valuable chemical transformations that include cyclopropanation, furanylation, C−H amination, and aziridination reactions.[24−28] The chemistry appears to involve carbene or nitrene transfer from a Co^{III} porphyrin intermediate. The electronic and steric nature of the porphyrin ligand has a significant influence on the selectivity of these reactions.[25,29]

Received: March 20, 2015
Published: June 2, 2015

DOI: 10.1021/acs.inorgchem.5b00636
Inorg. Chem. 2015, 54, 5864−5873

The aforementioned catalytic applications thus further merit the development of new macrocyclic cobalt compounds.

We herein describe the synthesis and characterization of an electron transfer series of cobalt compounds coordinated by the redox-active macrocyclic biquinazoline ligand, Mabiq[30] (Scheme 1). The synthesis and electronic structure studies of

Scheme 1

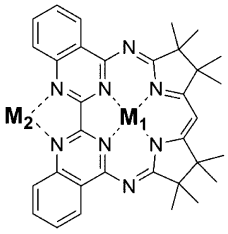

zinc- and iron-containing Mabiq complexes were reported previously.[31] These prior studies established the redox activity of the macrocycle, which is capable of accepting one electron via π^* orbitals of the diketiminate unit. In fact, experimental and computational data illustrated that the low-valent, *formally* Fe^{I} compound, Fe(Mabiq), was in actuality an intermediate-spin Fe^{II} compound, in which the iron ion is antiferromagnetically coupled to a Mabiq-centered radical.[31]

In light of findings from studies with the iron-containing complexes, we were eager to explore the coordination chemistry of Mabiq with cobalt. Electrochemical studies, detailed in this work, reveal that the Mabiq ligand supports formal cobalt valencies of 0 → 3+. We have successfully isolated the monometallic Co^{I}, Co^{II}, and Co^{III} forms in this redox series. In addition, we have isolated for the first time a bimetallic Mabiq compound, Co_2(Mabiq)Cl_3. The latter compound attests to the ability of the macrocyclic biquinazoline ligand to coordinate a second metal ion. The results of electronic structure studies on the series of macrocyclic cobalt compounds are presented. The work represents the first chapter in ongoing studies concerning the properties and reactivity of cobalt-Mabiq compounds.

EXPERIMENTAL SECTION

General Procedures. $CoCl_2$ and $CoCl_2{\cdot}6H_2O$ were purchased from Strem Chemicals, phosphorus pentachloride and phosphorus oxychloride were purchased from Alfa Aesar, and *N*,*N*-dimethylformamide (DMF) was purchased from AGTC Bioproducts. All other reagents were purchased from Sigma-Aldrich and used as received, except tetrabutylammonium hexafluorophosphate, which was recrystallized multiple times using ethanol. Metal compounds were synthesized in an inert atmosphere, under nitrogen, using anhydrous solvents. Solvents were dried by passage over activated alumina columns and stored over activated 3 or 4 Å molecular sieves. CH_2Cl_2 was dried over phosphorus pentoxide and distilled under argon prior to use.

H(Mabiq) was synthesized as previously described,[30,31] with the following modification: 4,4′-dihydroxy-2,2′-biquinazoline was synthesized by heating oxalylbis(anthranilamide) in a round-bottomed flask, under vacuum, at ∼350 °C, using a heating mantle. The resultant dark-brown solid was recrystallized from DMF (61% yield), and the product was confirmed by a comparison of the IR data to previously reported data.[30]

*Co(Mabiq)Cl$_2$ (**1**).* $CoCl_2{\cdot}6H_2O$ (66 mg, 0.28 mmol) was added to an aerated solution of H(Mabiq) (100 mg, 0.18 mmol) and triethylamine (24 μL, 0.19 mmol) in CH_2Cl_2 (10 mL). The solution was left to stir overnight and filtered through Celite, and the solvent was removed in vacuo, leaving a dark-brown solid. The product was recrystallized by the slow evaporation of a solution of **1** in CH_2Cl_2 (97 mg, 0.14 mmol, 78% yield).

Anal. Calcd for $C_{34}H_{35}Cl_4CoN_8$: C, 53.99; H, 4.66; N, 14.81. Found: C, 53.85; H, 4.71; N, 14.74. ^{1}H NMR (400 MHz, $CDCl_3$): δ 9.19 (dd, *J* = 8.3 and 0.8 Hz, 2H), 8.53 (d, *J* = 8.3 Hz, 2H), 8.10 (ddd, *J* = 8.5, 7.0, and 1.5 Hz, 2H), 7.89 (ddd, *J* = 8.2, 7.0, and 1.1 Hz, 2H), 6.49 (s, 1H), 1.51 (s, 12H), 1.48 (s, 12H). ^{13}C NMR (101 MHz, $CDCl_3$): δ 186.8, 177.9, 159.3, 156.7, 151.1, 135.7, 129.5, 129.2, 126.5, 124.2, 94.1, 51.9, 51.7, 24.3, 23.4. ASAP-MS(+): *m*/*z* 670 ($[M]^+$), 635 ($[M - Cl]^+$), 600 ($[M - 2Cl]^+$). UV−vis [λ_{max}, nm (ε, M^{-1} cm^{-1}), in CH_2Cl_2]: 273 (8.0×10^4), 322 (3.5×10^4), 381 (2.3×10^4), 432 (8.0×10^3), 484 (1.2×10^4), 514 (2.7×10^4). IR (cm^{-1}): 2978 w, 2930 w, 1603 m, 1572 m, 1561 m, 1510 s, 1488 m (sh), 1463 s, 1409 m, 1364 s, 1322 w, 1302 w, 1268 m, 1257 w (sh), 1232 m, 1199 w (sh), 1190 w, 1166 s, 1125 m, 1092 s, 1065 s, 1032 m (sh), 1000 m (sh), 963 m, 910 w, 893 m, 878 w, 866 w, 826 m, 813 w, 778 s, 758 m, 737 m (sh), 728 s, 718 m (sh), 697 m, 687 s, 663 w, 638 w, 628 m, 610 s.

*Co(Mabiq)Cl (**2**).* $CoCl_2$ (24 mg, 0.18 mmol) was added to a solution of H(Mabiq) (100 mg, 0.18 mmol) and triethylamine (24 μL, 0.19 mmol) in CH_2Cl_2 (10 mL). The solution was stirred overnight, the resultant green solution was filtered through Celite, and the solvent was removed in vacuo, leaving a dark-green solid (107 mg, 94.4% yield). Single crystals were obtained by the slow evaporation of a concentrated solution of **2** in CH_2Cl_2.

Anal. Calcd for $C_{33}H_{33}CoClN_8$: C, 62.31; H, 5.23; N, 17.62. Found: C, 62.19; H, 5.39; N, 17.52. ASAP-MS(+): *m*/*z* 601 ($[M - Cl]^+$), 543 ($[M - CoCl]^+$). UV−vis [λ_{max}, nm (ε, M^{-1} cm^{-1}), in MeOH]: 253 (2.9×10^4), 271 (2.2×10^4), 318 (1.9×10^4), 348 (1.7×10^4), 427 (7.0×10^3), 442 (7.2×10^3), 480 (3.6×10^3), 576 (2.1×10^3), 618 (2.2×10^3), 668 (1.7×10^3). IR (cm^{-1}): 2973 w, 1597 m, 1571 s, 1558 m (sh), 1544 w (sh), 1509 s, 1484 m, 1461 s, 1412 m, 1365 m, 1339 w, 1324 w, 1302 w, 1296 w (sh), 1270 m, 1255 w, 1242 m, 1195 w, 1167 m, 1123 s, 1097 vs, 1078 vs, 1031 w, 1017 w, 1006 w, 966 w, 958 w, 893 w, 866 w, 813 w, 811 w, 780 s, 763 m, 736 m, 719 w (sh), 702 w (sh), 668 m, 675 w, 663 w, 646 w, 634 w, 630 w, 611 m.

*Co$_2$(Mabiq)Cl$_3$ (**3**).* $CoCl_2$ (103 mg, 0.79 mmol) was added to a solution of H(Mabiq) (200 mg, 0.37 mmol) and triethylamine (48 μL, 0.38 mmol) in tetrahydrofuran (THF; 10 mL). The mixture was stirred overnight, and the resultant green precipitate was filtered and washed with THF (3 × 1 mL) and CH_2Cl_2 (3 × 1 mL) to give the dark-green solid **3** (269 mg, 95% yield).

Anal. Calcd for $C_{33}H_{33}Co_2Cl_3N_8$: C, 51.75; H, 4.34; N, 14.63. Found: C, 51.75; H, 4.28; N, 14.48. ASAP-MS(+): *m*/*z* 601 ($[M - CoCl_3]^+$). UV−vis [λ_{max}, nm (ε, M^{-1} cm^{-1}), in MeOH]: 253 (5.1×10^4), 271 (4.2×10^4), 318 (3.7×10^4), 348 (3.0×10^4), 427 (1.5×10^4), 442 (1.6×10^4), 480 (7.4×10^3), 576 (4.5×10^3), 618 (4.6×10^3), 668 (3.5×10^3). IR (cm^{-1}): 2967 w, 1560 s, 1502 m, 1488 m, 1474 s (sh), 1460 s, 1431 m (sh), 1409 s, 1378 m, 1362 m, 1306 w, 1276 w, 1257 w, 1228 m, 1200 w, 1169 m, 1125 m, 1094 s, 1072 s, 974 w, 956 w, 897 m.

*Co(Mabiq) (**4**).* Cp_2Co (12.7 mg, 0.067 mmol) was added to a suspension of **2** (42.7 mg, 0.067 mmol) in THF (5 mL), upon which the mixture immediately turned a deep purple. The reaction mixture was stirred for 2 h and filtered through Celite. The solvent was subsequently removed in vacuo, yielding a purple solid (35 mg, 87% yield). Single crystals were obtained by the slow evaporation of a concentrated solution of **4** in THF or, alternatively, by the slow diffusion of pentane into a solution of **4** in THF.

Anal. Calcd for $C_{33}H_{33}CoN_8$: C, 65.99; H, 5.54; N, 18.66. Found: C, 66.16; H, 5.62; N, 18.34. ^{1}H NMR (400 MHz, THF-d_8): δ 9.06 (dd, *J* = 8.2 and 0.9 Hz, 2H), 8.37 (d, *J* = 8.1 Hz, 2H), 8.19 (td, *J* = 7.6 Hz, 2H), 7.64 (td, *J* = 7.6 Hz, 2H), 7.54 (s, 1H), 1.55 (s, 12H), 1.39 (s, 12H). ASAP-MS(+): *m*/*z* 600 ($[M]^+$). UV−vis [λ_{max}, nm (ε, M^{-1} cm^{-1}), in THF]: 268 (4.4×10^4), 324 (3.5×10^4), 335 (3.7×10^4), 392 (1.9×10^4), 403 (2.4×10^4), 523 (1.3×10^4), 533 (1.4×10^4), 913 (2.8×10^3), 1048 (2.0×10^3), 1210 (2.1×10^3). IR (cm^{-1}): 2971 w, 2906 w, 1608 w, 1591 w (sh), 1564 m, 1548 m, 1506 m, 1480 m, 1463 w, 1446 m, 1414 m, 1388 w, 1374 m, 1364 m (sh), 1354 m, 1325 w, 1280 m, 1253 w, 1222 m, 1187 vw, 1164 m, 1149 m, 1136 s, 1109

DOI: 10.1021/acs.inorgchem.5b00636
Inorg. Chem. 2015, 54, 5864−5873

Scheme 2. Synthesis of Compounds 1−4

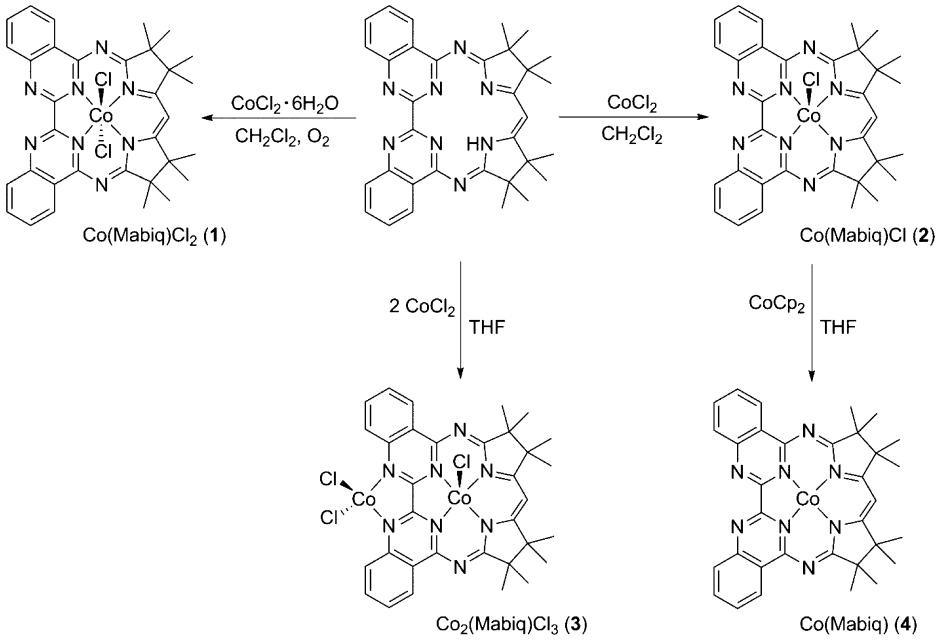

m (sh), 1016 w, 967 w, 954 vw, 896 w, 867 m, 819 w (sh), 813 m, 792 vw, 765 vs, 748 s, 696 m, 690 m, 673 m, 632 m, 625 m, 612 m.

Physical Measurements. NMR spectra were recorded on a Bruker Avance-400 (400 MHz ^{1}H and 100 MHz ^{13}C) spectrometer. Electronic spectra were recorded on a PerkinElmer Lambda 900 spectrophotometer. Diffuse-reflectance spectra were obtained by fixed-angle oblique illumination of the sample using an Energetiq LDLS EQ-99 broad-band lamp and collection perpendicular to the face of the sample using an Ocean Optics Maya Pro 2000 spectrometer. Data were recorded using the Ocean Optics software, and integration times were adjusted to afford maximum response of the spectrometer without saturation of the detector. NaCl was used as the white standard. Mass spectrometry (MS) spectra were measured using a LCT Premier XE mass spectrometer and an Acquity UPLC (Waters Ltd., Elstree, Borehamwood, U.K.). IR spectra were recorded using a PerkinElmer Spectrum 100 spectrometer. Microanalyses were performed at London Metropolitan University or at the microanalytical laboratory of the TUM. Electrochemical measurements were carried out using a Palm Emstat2 potentiostat with a three-electrode cell equipped with a platinum auxiliary electrode, a glassy carbon working electrode, and either a $Ag/AgNO_3$ or a platinum reference electrode (CH_2Cl_2). Potentials are reported with reference to an internal standard ferrocenium/ferrocene ($Fc^{+/0}$). Magnetic susceptibility data (2−290 K) were recorded using a SQUID magnetometer (MPMS7, Quantum Design) in a 1 T external field. Data were corrected for underlying diamagnetism using tabulated Pascal's constant and fit using julX (Dr. E. Bill). Electron paramagnetic resonance (EPR) measurements were carried out at the EPSRC National UK EPR Facility and Service in the Photon Science Institute at The University of Manchester. X-band spectra were collected on Bruker EMX and EMX Micro spectrometers, and simulations were performed using Bruker's *Xsophe* software package.[32]

Crystallography. Single-crystal X-ray data for **1** and **2** were collected at 120.0(1) K on a Bruker D8Venture diffractometer [PHOTON-100 CMOS detector, IμS microsource, focusing mirrors, λ(Mo Kα), and λ = 0.71073 Å] and on a Rigaku Saturn 724+ diffractometer (compound **4**) at station I19 of the Diamond Light Source synchrotron (undulator, λ = 0.6889 Å, ω scan, and 1.0° frame^{-1}) and processed using Bruker *APEXII* software. The temperature of the samples was maintained by Cryostream (Oxford Cryosystems) open-flow nitrogen cryostats. All structures were solved by direct methods and refined by full-matrix least squares on F^2 for all data using *Olex2*[33] and *SHELXTL*[34] software. All nondisordered non-hydrogen atoms were refined anisotropically, hydrogen atoms in structures **2** and **4** were refined isotropically, hydrogen atoms in structure **1** were placed in the calculated positions and refined in riding mode.

Density Functional Theory (DFT) Calculations. All DFT calculations were performed with the *ORCA* program package.[35] The geometry optimizations of the complexes were performed at the B3LYP level of DFT.[36−38] The all-electron Gaussian basis sets were those developed by the Ahlrichs group.[39,40] Triple-ζ-quality basis sets TZV(P) with one set of polarization functions were used on the metals and on the atoms directly coordinated to the metal center.[41] For the carbon and hydrogen atoms, slightly smaller polarized split-valence SV(P) basis sets were used, which were of double-ζ quality in the valence region and contained a polarizing set of d functions on the non-hydrogen atoms.[42] Auxiliary basis sets used to expand the electron density in the resolution-of-the-identity approach were chosen, where applicable, to match the orbital basis.[43,44] The self-consistent-field calculations were tightly converged (1×10^{-8} E_h in energy, 1×10^{-7} E_h in the density change, and 1×10^{-7} in the maximum element of the DIIS error vector). The geometry optimizations for all complexes were carried out in redundant internal coordinates without imposing symmetry constraints. In all cases, the geometries were considered converged after the energy change was less than 5×10^{-6} E_h, and the gradient norm and maximum gradient element were smaller than 1×10^{-4} and 3×10^{-4} E_h Bohr^{-1}, respectively, and the root-mean-square and maximum displacements of all atoms were smaller than 2×10^{-3} and 4×10^{-3} Bohr, respectively. Single-point calculations on the nonoptimized structures, using the coordinates obtained crystallographically, also were carried out using the B3LYP functional. The results of unrestricted (UKS) calculations were compared to those obtained using the broken-symmetry (BS)[45−47] approach, for calculations on both the optimized and nonoptimized geometries. Corresponding[48] and canonical orbitals and density plots were created using *GaussView*.[49]

RESULTS AND DISCUSSION

Synthesis and Characterization. The Co^{III}- and Co^{II}-Mabiq complexes were synthesized in straightforward reactions of the macrocyclic ligand with $CoCl_2$ starting materials (Scheme 2). For the synthesis of $Co(Mabiq)Cl_2$ **1**, we initially followed a protocol similar to that employed for the synthesis of $Co(Mabiq)CN_2$,[30] using $CoCl_2 \cdot 6H_2O$ as the source of the

DOI: 10.1021/acs.inorgchem.5b00636
Inorg. Chem. 2015, 54, 5864−5873

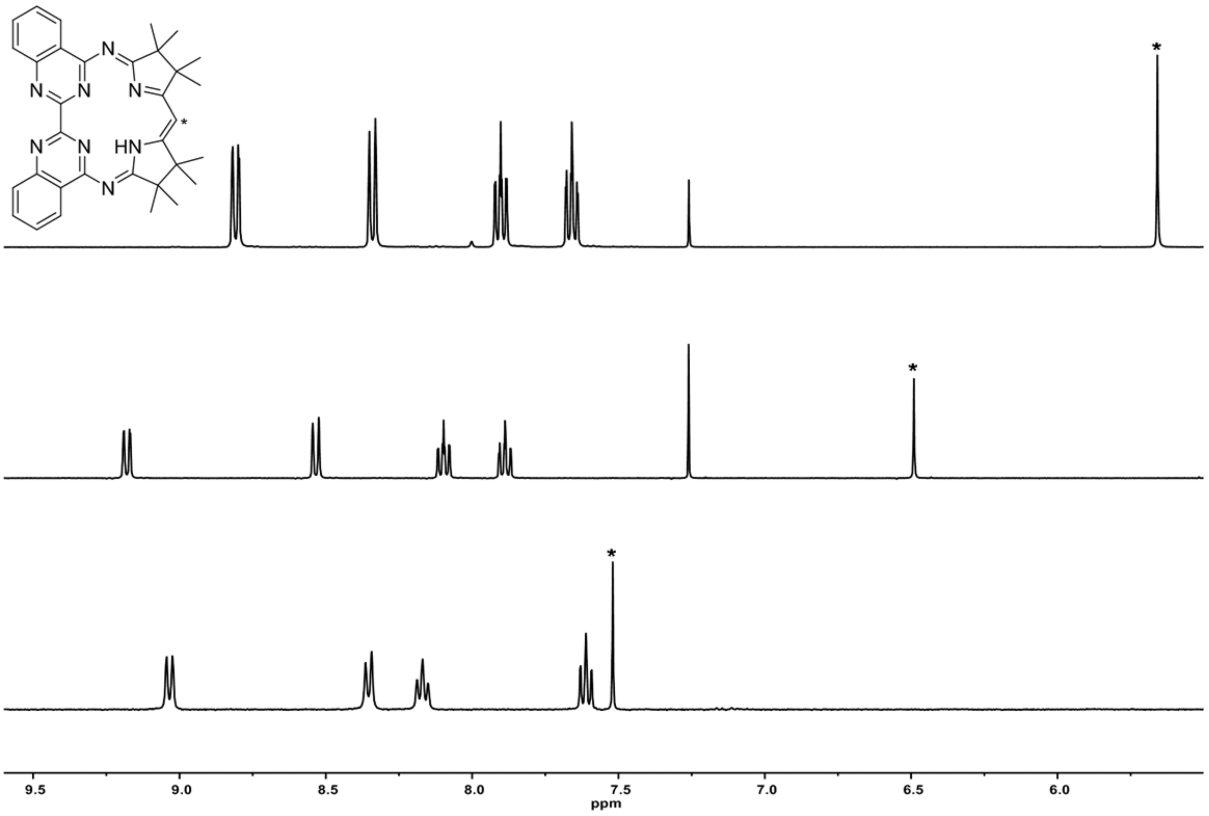

Figure 1. ^{1}H NMR spectra of H(Mabiq) (top, $CDCl_3$), **1** (middle, $CDCl_3$), and **4** (bottom, THF-d_8), showing the aromatic protons and diketiminate proton (*) for comparison.

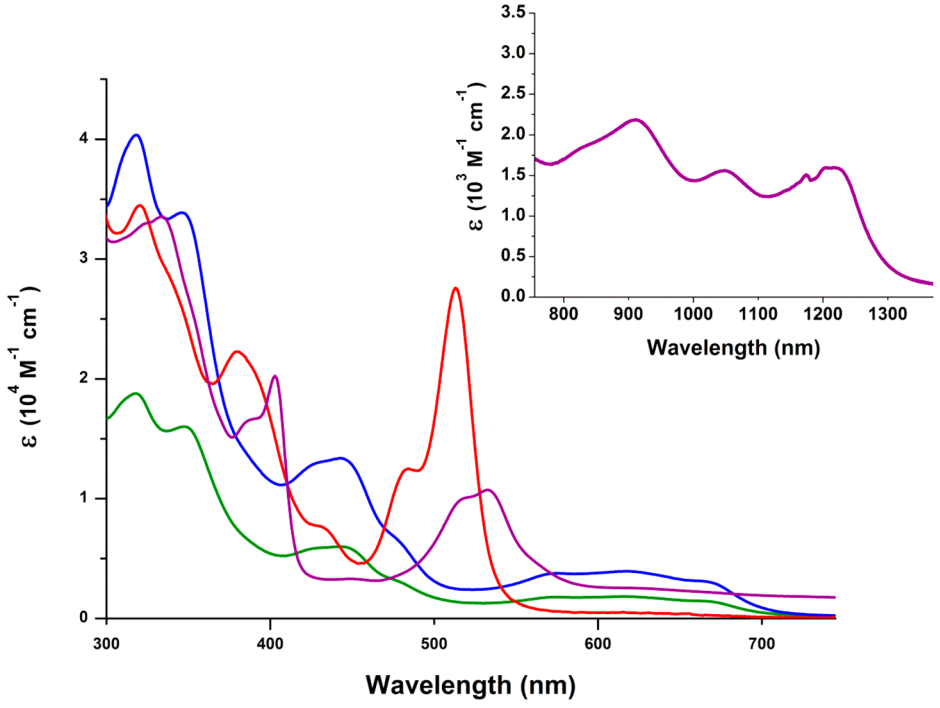

Figure 2. Electronic spectra of **1** (red, CH_2Cl_2), **2** (green, CH_3OH), **3** (blue, CH_3OH), and **4** (purple, THF). Inset: NIR region of the spectrum of **4**.

metal ion and H_2O_2 as an oxidant. However, higher product yields were obtained by simply allowing H(Mabiq) and $CoCl_2 \cdot 6H_2O$ to react in aerated CH_2Cl_2 solutions, with O_2 as the oxidant. The ^{1}H NMR spectrum of the diamagnetic **1** shows an upfield shift of the aromatic and diketiminate C−H protons, compared to the spectrum of the free H(Mabiq) ligand (Figure 1), attributable to the presence of the Co^{III} ion in the macrocyclic cavity. The electronic spectrum of **1** (Figure 2),

DOI: 10.1021/acs.inorgchem.5b00636
Inorg. Chem. 2015, 54, 5864−5873

with absorption bands at λ_{max} = 484 and 514 nm, resembles those of Zn(Mabiq)Cl (λ_{max} = 471 and 502 nm) and Co(Mabiq)$(CN)_2$ (λ_{max} = 502 and 536 nm).[30,31] The features in the visible region of the latter complex were ascribed to Mabiq $\pi-\pi^*$ transitions by von Zelewsky, and the energy was deemed dependent on the charge of the coordinated metal ion.[30] The positions of these absorption bands among the spectra of **1**, Zn^{II}(Mabiq)Cl, Co^{III}(Mabiq)$(CN)_2$, and Fe^{III}(Mabiq)Cl_2 (λ_{max} = 524 nm) appear to be consistent with this conclusion.

von Zelewsky's original motivation for the synthesis of the biquinazoline ligand was to design a bimetallic complex with photocatalytic properties.[30] The Mabiq ligand offers two potential metal-coordination sites, as depicted in Scheme 1. The primary coordination site is furnished by the N_4 cavity, but the external diimine moiety of the bipyrimidine provides an additional metal-binding site. The binuclear complexes targeted by von Zelewsky were never subsequently reported. We also were not able to isolate or obtain evidence for the formation of binuclear products in prior studies pertaining to the coordination chemistry of Mabiq with iron. However, we have now generated both mono- and bimetallic cobaltous complexes, Co(Mabiq)Cl (**2**) and Co_2(Mabiq)Cl_3 (**3**), upon the reaction of H(Mabiq) with either 1 or 2 equiv of anhydrous $CoCl_2$, respectively. Complex **3** offers, for the first time, evidence for the ability to coordinate a metal ion to the secondary Mabiq binding site.

The solid-state composition of the bimetallic **3** was verified by elemental analysis. On the basis of elemental analysis, the known structure of **2**, and magnetic susceptibility data for both compounds (vide infra), we propose the structure of **3** as shown in Scheme 2: the coordination environment of the metal ion in the primary Mabiq binding site is akin to that in **2**, while the second cobaltous site is four-coordinate tetrahedral, ligated by two chloride ions and the bipyrimidine nitrogen atoms. Minor differences in the visible−near-IR (NIR) region are apparent between the solid-state spectra of **2** and **3** (Figure S3 in the Supporting Information, SI), and the solid-state IR spectra of the two compounds also exhibit several distinctive bands in the fingerprint region (Figure S4 in the SI). Compounds **2** and **3** have markedly different solubilities in CH_2Cl_2, in which only the monometallic complex is soluble, but both compounds are soluble in CH_3OH. Surprisingly, the solution absorption spectra of **2** and **3** in CH_3OH are superimposable (Figure 2), exhibiting identical transitions in the UV−NIR region (250−900 nm), which differ only in the values of their extinction coefficients. The similarity of the spectra suggests that the $CoCl_2$ moiety occupying the outer diimine site of **3** may only be weakly bound, dissociating in solution.

The final compound in this series, the low-valent Co(Mabiq) (**4**), was generated upon reduction of **2** with $CoCp_2$ in THF. The ^{1}H NMR spectrum of the diamagnetic compound in THF-d_8 is shown in Figure 1. A notable feature in the NMR spectrum is the diketiminate C−H proton signal, which appears at 7.54 ppm, significantly upfield in comparison to its position in the spectrum of the diamagnetic Co^{III}-, Fe^{II}-, and Zn^{II}-Mabiq complexes.[31] The solution electronic spectrum of purple **4** in THF exhibits the common $\pi-\pi^*$ transitions at λ_{max} = 392 and 403 nm, as well as absorption bands at λ_{max} = 523 and 533 nm, which we tentatively assign as metal-to-ligand charge-transfer transitions. In addition, multiple features can be seen in the NIR region (750−1300 nm, Figure 2). In this respect, the spectrum of **4** closely resembles that of Co^I cobalamin.[50] The absorption spectrum of the superreduced vitamin B_{12} also displays low-energy transitions between 500 and 1100 nm, which were assigned as Co 3d → corrin π^* excitations, based on time-dependent DFT computational studies. The relevant vitamin B_{12} π^* orbitals are predominantly localized on the diketiminate group of the corrin ring. It is therefore not unreasonable that a similar Co → Mabiq transition, involving the π^* orbitals of the redox-active diketiminate functionality, might account for the NIR transitions in the spectrum of **4**. However, in-depth computational analysis will be required to detangle the various possible contributions to these low-energy bands.[51]

Electrochemistry. The cyclic voltammograms (CV) for complexes **1**−**4** are shown in Figure 3. The CVs of **1** and **2** are

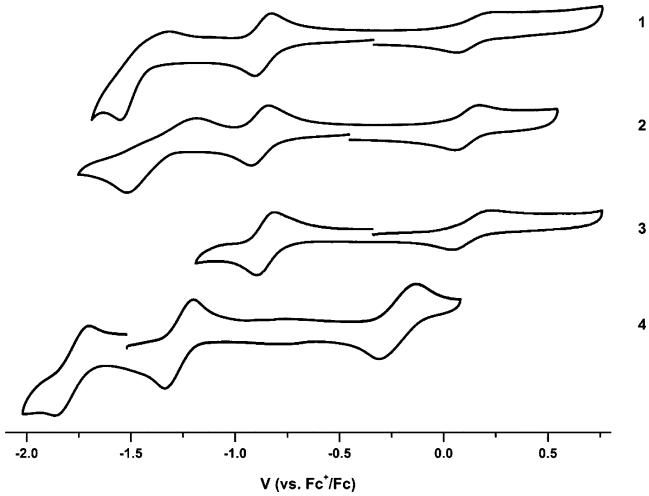

Figure 3. CVs of **1**−**4** (0.2 V s^{-1}; 0.1 M $[N(n\text{-}Bu)_4]PF_6$; that of **4** in THF and all others in CH_3OH).

very similar. In each case, an irreversible redox event occurs at $E_{1/2}$ = ∼0.1 V (vs $Fc^{+/0}$) that can be assigned to the Co^{III}/Co^{II} couple. The oxidative process is followed by a reversible one-electron reduction at $E_{1/2}$ = ∼−0.9 V and a second irreversible reductive event at E_a = ∼−1.5 V (Table 1). All three redox

Table 1. Reduction Potentials (V vs $Fc^{+/0}$) of 1−4 (the Oxidation State Represents the Formal Metal Valency)

	$E_{1/2}$ (Co^{III}/Co^{II})	$E_{1/2}$(Co^{II}/Co^{I})	$E_{1/2}$(Co^{I}/Co^{0})
1	0.14	−0.86	E_a = −1.53; E_c = −1.33
2	0.11	−0.88	E_a = −1.51; E_c = −1.22
3	0.12	−0.85	
4	−0.22	−1.27	−1.78

events, likewise, are apparent in the CV of **4** (in THF) but are shifted to more negative potentials, and all appear to be reversible.[52] The presence of the axial ligand clearly has a substantial effect on the electrochemical potentials.

Ligand-centered reduction, as established for the Zn- and Fe-Mabiq complexes, occurred at potentials of −0.9 to −1.5 V.[31] The second redox process in the CVs of **1**, **2**, and **4**, formally corresponding to the Co^{II}/Co^{I} couple, thus can be attributed to the formation of either a Co^{I}(Mabiq) or a Co^{II}(Mabiq$^{\bullet}$) species. The ensuing redox event, again *formally* described by Co^0 formation, likely entails the formation of $[Co^{I}(Mabiq^{\bullet})]^-$,

DOI: 10.1021/acs.inorgchem.5b00636
Inorg. Chem. 2015, 54, 5864−5873

in which both the metal ion and ligand are one-electron reduced.

The presence of an additional Co^{II} ion in the bimetallic **3** has a negligible effect on the electrochemistry, compared to the redox behavior of the monometallic compounds. Redox processes apart from those ascribed to the cobalt ion in the macrocyclic cavity are not observed in the range of −1.2 to +0.8 V. The potentials of the Co^{III}/Co^{II} and Co^{II}/Co^{I} couples are equivalent to those of **1** and **2**. The Co^{I}/Co^{0} couple is indiscernible though, and scanning at potentials more negative than −1.2 V led to the appearance of new redox waves (Figure S5 in the SI). The discrepancies in the redox behavior of **2** and **3** intimate different chemical compositions for the two cobaltous products in solution. Nevertheless, the lack of any redox couples obviously associated with the (bipyrimidine)-$CoCl_2$ moiety is surprising. Redox deactivation by a neighboring metal ion has been observed previously in bimetallic complexes[53] and may be operational in our system. However, the presence of any free $CoCl_2$ in solution, stemming from the dissociation of **3**, also would complicate the electrochemistry. As we presently cannot confirm the solution-state composition of **3**, we are unable to draw any further conclusions from the CV regarding the influence of the second cobalt site.

Solid-State Structures. Single crystals were obtained for the monometallic complexes **1**, **2**, and **4** (Table 2), and the solid-state structures are shown in Figure 4. The coordination number of the cobalt complexes decreases according to the formal metal valency: complex **1** is six-coordinate pseudooctahedral, complex **2** adopts a five-coordinate square-pyramidal geometry, whereas complex **4** is four-coordinate square-planar. In all structures, the dihydropyrrole backbone of the macrocycle is arranged in the "syn" conformation, as previously denoted for metal-Mabiq complexes.[30,31] The bipyrimidine unit of the Mabiq ligand exhibits varying degrees of distortion among the series of compounds. The macrocyclic ligand is severely buckled in **4**, which also results in a ∼6° difference in coplanarity between the two pyrimidine groups. The torsion angle of the C−C bond joining the quinazoline unit is significantly reduced in **2** (1.8°) and may account, in part, for the existence of both the mono- and binuclear forms of the cobaltous complex.

Table 2. Crystallographic Data

	$1{\cdot}CH_2Cl_2$	$2{\cdot}2CH_2Cl_2$	**4**
empirical formula	$C_{34}H_{35}N_8Cl_4Co$	$C_{35}H_{37}N_8Cl_5Co$	$C_{33}H_{33}N_8Co$
fw	756.43	805.91	600.60
cryst syst	triclinic	monoclinic	orthorhombic
space group	$P\bar{1}$	$P2_1/c$	$Pbca$
a (Å)	10.0493(7)	11.6266(8)	10.199(3)
b (Å)	18.586(1)	21.949(2)	20.351(6)
c (Å)	19.448(1)	15.014(1)	26.781(8)
α (deg)	101.466(2)	90.00	90.00
β (deg)	104.309(2)	108.541(2)	90.00
γ (deg)	103.074(2)	90.00	90.00
volume (Å^3)	3301.4(4)	3632.4(4)	5559(3)
Z	4	4	8
ρ_{calc} (mg mm^{-3})	1.522	1.474	1.435
μ (mm^{-1})	0.883	0.879	0.608
F(000)	1560.0	1660.0	2512.0
reflns collected	55117	50205	36358
indep reflns/R_{int}	18354/0.0331	9196/0.0519	4231/0.0984
data/restraints/ param	18354/6/866	9196/0/590	4231/0/511
GOF on F^2	1.027	1.011	1.054
final R1 indexes [$I \geq 2\sigma(I)$]	0.0393	0.0501	0.0484
final wR2 indexes (all data)	0.1024	0.1434	0.1267
$\Delta\rho_{min,max}$ (e Å^{-3})	0.81/−0.54	0.85/−1.21	0.35/−0.53

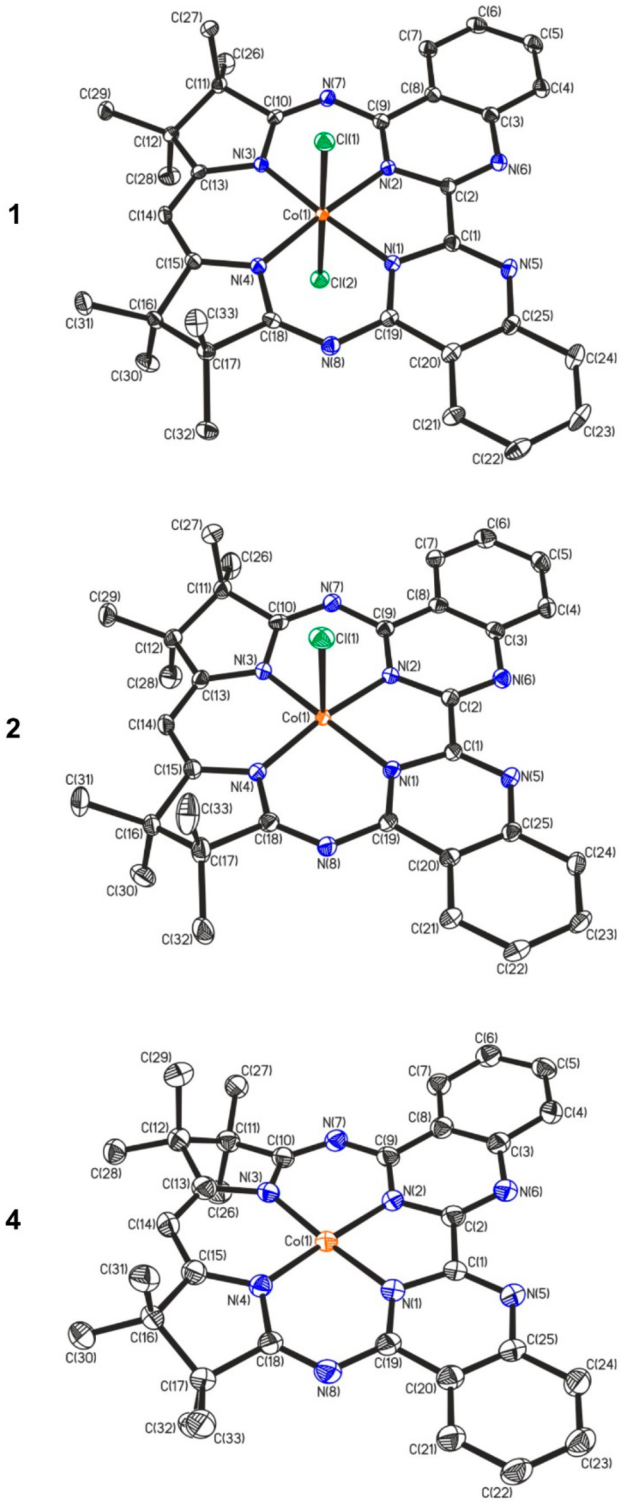

Figure 4. Molecular structures of **1**, **2**, and **4** (50% probability ellipsoids). Hydrogen atoms and solvent molecules omitted for clarity.

DOI: 10.1021/acs.inorgchem.5b00636
Inorg. Chem. 2015, 54, 5864−5873

The Co−N distances among the three monometallic complexes reflect the typical asymmetric metal coordination,[30,31] with slightly shorter bonds to the diketiminate nitrogen atoms versus to the bipyrimidine unit (Table 3).

Table 3. Select Bond Distances (Å) for 1, 2, and 4

	1	2	4
Co−N(1)	1.918(1)	1.918(2)	1.877(3)
Co−N(2)	1.924(1)	1.911(2)	1.878(3)
Co−N(3)	1.898(1)	1.892(2)	1.857(3)
Co−N(4)	1.903(1)	1.891(2)	1.864(3)
N(3)−C(13)	1.348(2)	1.356(3)	1.374(5)
C(13)−C(14)	1.378(2)	1.376(4)	1.381(6)
C(14)−C(15)	1.380(2)	1.386(4)	1.368(5)
N(4)−C(15)	1.344(2)	1.344(3)	1.368(5)
Co−Cl	2.2685(5), 2.2557(5)	2.4458(7)	

The average Co−N bond lengths of **1** and **2** are comparable (**1**, Co−N_{avg} = 1.91 Å; **2**, Co−N_{avg} = 1.90 Å). However, the metal−N bond distances of **4** are significantly shorter (Co−N_{avg} = 1.87 Å), denoting significant metal-to-ligand π-back-bonding. The bond lengths of the diketiminate unit of **4** also are noteworthy, considering that this component represents the redox-active functionality of the macrocycle. The average C−C bond distance of this unit is slightly shorter than the analogous bond lengths in **1** and **2**, whereas the C−N bonds are considerably longer. Similar bond distances were observed in the reduced Fe^{II}(Mabiq$^{\bullet}$) complex.[31] The structural data further highlight the issue regarding the most accurate description of the low-valent compound **4**: whether Co^{I}(Mabiq) or Co^{II}(Mabiq$^{\bullet}$).

Electronic Structures. The electronic structures of the paramagnetic mono- and bimetallic Co^{II} complexes, **2** and **3**, were examined using EPR spectroscopy and SQUID magnetometry. Magnetic susceptibility data for **2** (2−300 K, 1 T; Figure S6 in the SI) afford a temperature-independent μ_{eff} = 1.88 μ_B and g = 2.17, establishing an $S = {}^1/_2$ ground state for the Co^{II} complex. The X-band EPR spectrum recorded in a CH_2Cl_2/toluene solution at ambient temperature is indicative of a low-spin Co^{II} center (Figure S7 in the SI). Coupling to the ^{59}Co ($I = {}^7/_2$; 100% natural abundance) nucleus produces an eight-line hyperfine splitting of the electron-spin resonance. Successful simulation was achieved using g_{iso} = 2.204 and $A_{iso} = 55 \times 10^{-4}$ cm^{-1} and a Kivelson line-shape model that accounts for the uneven profile of the hyperfine lines brought about by motional tumbling of **2** in the solvent mixture.

At 30 K, the frozen solution spectrum is richly detailed with hyperfine structure (Figure 5). Simulation was achieved using g = (2.280, 2.280, 2.002) and $A\{^{59}Co\} = (35, 36, 111) \times 10^{-4}$ cm^{-1}. The axial splitting of the principal g and A values, where $g_\perp > g_\parallel \sim g_e$ and $A_\perp < A_\parallel$ are diagnostic of a ^{2}A ground-state term of a Co^{II} ion with a $(d_{xy,xz,yz})^6(d_{z^2})^1$ electron configuration. The magnitude of the g anisotropy is indicative of a five-coordinate low-spin Co^{II} ion and markedly different from that of a four-coordinate species.[54,55] Interestingly, the axially split spectrum is more akin to Co^{II} ions encapsulated by symmetric macrocycles such as porphyrins and phthalocyanines.[56−62] The removal of in-plane symmetry provided by corrins,[63,64] corroles,[65−68] and Schiff base macrocycles[69,70] introduces significant rhombicity in the g-values ($g_x > g_y$), which is seemingly negated by the diketiminate unit in Mabiq. The presence of a single apical Cl^- ligand is manifested in the additional hyperfine splitting of the parallel hyperfine lines to high field. Six of these features are visible, with the missing two overlapping with the perpendicular components to lower field. This structure was accommodated in the simulation with a coupling to the ^{35,37}Cl ($I = {}^3/_2$) nucleus of 25 × 10^{-4} cm^{-1}. Only the parallel contribution (A_z) is resolved in the spectrum, which has been observed for numerous Lewis base adducts of Co^{II} ions in an N_4 macrocycle.[63,68,71,72]

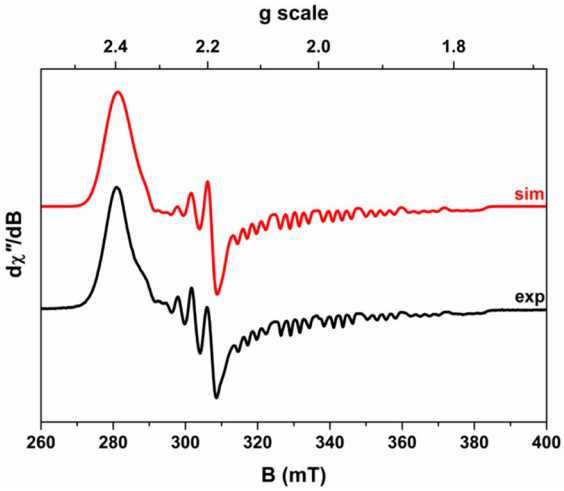

Figure 5. X-band EPR spectrum of **2** recorded in CH_2Cl_2/toluene at 30 K (experimental conditions: frequency, 9.3668 GHz; modulation, 0.5 mT; power, 0.63 mW). The experimental spectrum is shown in black and the simulation depicted by the red trace: g = (2.280, 2.280, 2.002); $A\{^{59}Co\} = (35, 36, 111) \times 10^{-4}$ cm^{-1}; $A\{^{35,37}Cl\} = (0, 0, 25) \times 10^{-4}$ cm^{-1}.

Magnetic susceptibility measurements for the dicobalt complex, **3**, show a temperature-independent magnetic moment from 50 to 300 K, yielding a value of μ_{eff} = 4.3 μ_B, which decreases below 50 K to a value of $\mu_{eff} \sim 3.8$ μ_B (Figure 6). The room temperature value of the magnetic moment is fully consistent with the presence of two Co^{II} ions in **3** with $S = {}^1/_2$ and $S = {}^3/_2$ ground states (the spin-only value for two uncoupled $S = {}^1/_2$ and $S = {}^3/_2$ ions is μ_{eff} = 4.24 μ_B for g = 2). The data were fit according to the following spin Hamiltonian:

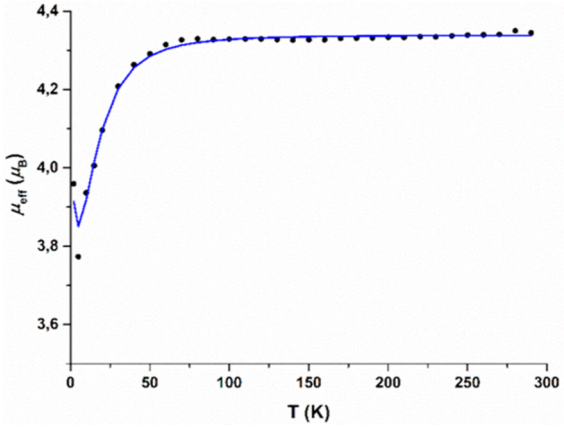

Figure 6. Temperature dependence of the magnetic moment μ_{eff}, μ_B, of a powdered sample of **3**. Filled circles are experimental data; the blue line represents the best fit: $S_1 = {}^3/_2$; $S_2 = {}^1/_2$; g_1 = 2.05; g_2 = 2.0; J_{12} = 0.47 cm^{-1}; $|D_2|$ = 20.37 cm^{-1}; TIP = 1500 × 10^{-6} cm^3 mol^{-1}.

DOI: 10.1021/acs.inorgchem.5b00636
Inorg. Chem. 2015, 54, 5864−5873

$$\hat{H} = -2J\hat{S}_1\cdot\hat{S}_2 + g\mu_B(\hat{S}_1 + \hat{S}_2)\cdot\vec{B} + \sum_{i=1,2} D\left[\hat{S}_z^{\,2} - \frac{1}{3}S_i(S_i+1) + \frac{E}{D}(\hat{S}_{x,i}^{\,2} - \hat{S}_{y,i}^{\,2})\right]$$

including exchange coupling (J) and zero-field-splitting (ZFS) terms, with $S_1 = {}^1/_2$ and $S_2 = {}^3/_2$. The data were best fit with $g_1 = 2.05$, $g_2 = 2.0$, $J = 0.47$ cm^{-1}, and $|D_2| = 20.37$ cm^{-1}. The miniscule exchange coupling constant denotes weak coupling between the two Co^{II} centers. The value of the ZFS for the high-spin Co^{II} ion is consistent with the values observed for tetrahedral cobaltous compounds, which can range widely depending on the ligand field and degree of distortion from tetrahedral geometry.[73−77] The data fully support the solid-state bimetallic assignment of **3** previously surmised: the low-spin ($S = {}^1/_2$) cobaltous ion resides in the macrocylic cavity, additionally ligated by an axial chloride ligand, whereas the second cobaltous site adopts the expected high-spin $S = {}^3/_2$ configuration expected for a d^7 ion in a tetrahedral environment.

The fluid-solution EPR spectrum of **3** in methanol is essentially identical with that for **2** (Figure S8 in the SI) with $g_{iso} = 2.196$ and $A_{iso} = 49 \times 10^{-4}$ cm^{-1}. The overall profile is slightly more askew than that for **2**, which is a consequence of the increased mass of the molecule or simply a change of the solvent. The hyperfine pattern reveals that observable resonances can arise from a unique single spin only, presumably the square-pyramidal $S = {}^1/_2$ Co^{II} ion, because the electron-spin relaxation in the high-spin center precludes its appearance in a fluid solution. The frozen-solution spectrum recorded in a CH_3OH/toluene solution at 10 K consists of a broad signal at ∼120 mT attributed to an $S = {}^3/_2$ species and a second signal at ∼300 mT consistent with the assumed spin doublet observed at room temperature (Figure S9 in the SI). This spectrum is additional evidence for the dissociation of the bimetallic **3** in solution, as the spectral profile cannot be reproduced using the spin Hamiltonian parameters obtained from fitting of the magnetic susceptibility data (Figure 6). The high-field signal exhibits six peaks readily ascribed to $A_{\|}$ of the low-spin Co^{II} center (the remaining two are obscured by the perpendicular components), with a coupling nearly identical with that measured for **2** (vide supra). Notably these peaks lack the superhyperfine splitting to the apical Cl$^-$ ligand, suggesting that this has been replaced by either methanol or water. However, they are too weak to be associated with the bulk of the signal centered at ∼300 mT, whose four prominent peaks cannot be readily interpreted at this stage. Dissociation liberates the high-spin Co^{II} ion, which presumably generates the broad signal at ∼120 mT. This subspectrum has been simulated as an $S = {}^3/_2$ species with $D \gg h\nu$, yielding axial $g = (2.35, 2.35, 2.58)$ with a small rhombic contribution to the ZFS of $E/D = 0.03$ (dashed line, Figure S9 in the SI). The simulation employed large Gaussian linewidths, $W = (450, 450, 1000) \times 10^{-4}$ cm^{-1}, and E/D strain ($\sigma_{E/D} = 0.22$). These parameters match those of related tetrahedral Co^{II} compounds.[78]

The ambiguity concerning the oxidation state of the cobalt ion in **4** prompted us to carry out DFT investigations (B3LYP) of the low-valent compound. Calculations were carried out using either the UKS or BS approach on the geometry-optimized structure. The experimentally derived and geometry-optimized structures differed slightly with respect to the extent of distortion of the macrocyclic ligand (Tables 3 and S1−S3 in the SI). Therefore, the results were further compared to single-point energy calculations performed on the nonoptimized, crystallographically determined structure of **4** to examine whether minor geometric perturbations would bias the electronic structure. The relevant DFT-derived, metal-based molecular orbitals from calculations on either structure were nearly identical in character, although variations in their relative energies were occasionally observed (Figures 8 and S10−S11 in the SI). A lower-energy solution was consistently provided by the BS approach (∼2.4 kcal mol^{-1}) versus the UKS calculation, which converged to a closed-shell solution.

The BS calculations describe a Co^{II}(Mabiq$^{\bullet}$) electronic structure for **4**. The DFT-derived spin-density map (Figure 7)

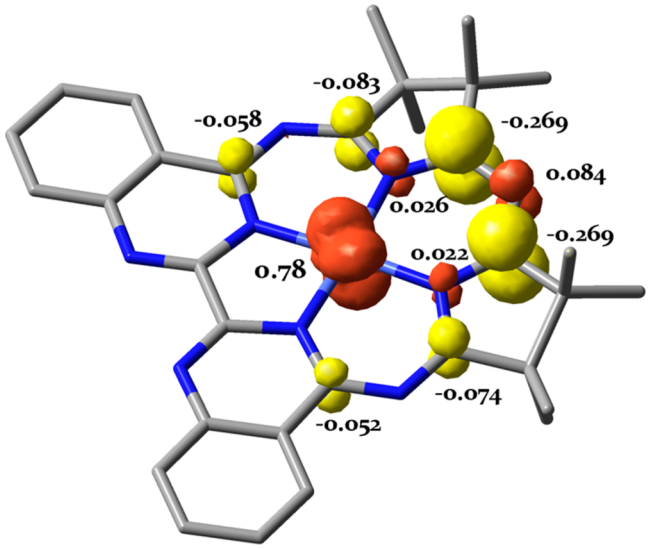

Figure 7. DFT-derived (B3LYP) spin-density plot for **4** [BS(1,1) calculation on the geometry-optimized structure] based on Löwdin population analysis.

depicts one unpaired spin on the cobalt center and one unpaired spin of opposite sign on the Mabiq ligand. The qualitative molecular orbital diagram (Figure 8) depicts a singly occupied metal-based orbital (d_{xz}) of α spin that has a spatial overlap of 0.57 with a ligand-centered singly occupied molecular orbital, occupied by the electron of β spin. Analogous to the findings from computational studies on Fe^{II}(Mabiq$^{\bullet}$) and Zn^{II}(Mabiq$^{\bullet}$), the ligand-centered electron is localized on the diketiminate component of the macrocycle. Nonetheless, the small energy difference between the BS and UKS solutions precludes an unambiguous assignment of the oxidation levels in **4**, whose electronic structure is best represented by the resonance forms Co^{I}(Mabiq) ↔ Co^{II}(Mabiq$^{\bullet}$).

CONCLUSIONS

The coordination chemistry of Mabiq with cobalt is similar to that of its neighboring transition metal, iron, likewise allowing for isolation of a three-electron series of monometallic compounds (**1**, **2**, and **4**). The metal ion in the square-pyramidal environment of **2** adopts a low-spin $S = {}^1/_2$ configuration and, judging from the EPR data, is a genuine d^7 cobaltous compound. This contrasts with the isoelectronic Fe(Mabiq), in which the macrocyclic ligand is in the reduced (Mabiq$^{\bullet}$)$^-$ form and coordinates an $S = 1$ ferrous ion. Compound **4** is the most interesting among the monometallic cobalt compounds. As noted previously, the Co^{I} forms of related macrocyclic complexes have garnered attention due to

DOI: 10.1021/acs.inorgchem.5b00636
Inorg. Chem. 2015, 54, 5864−5873

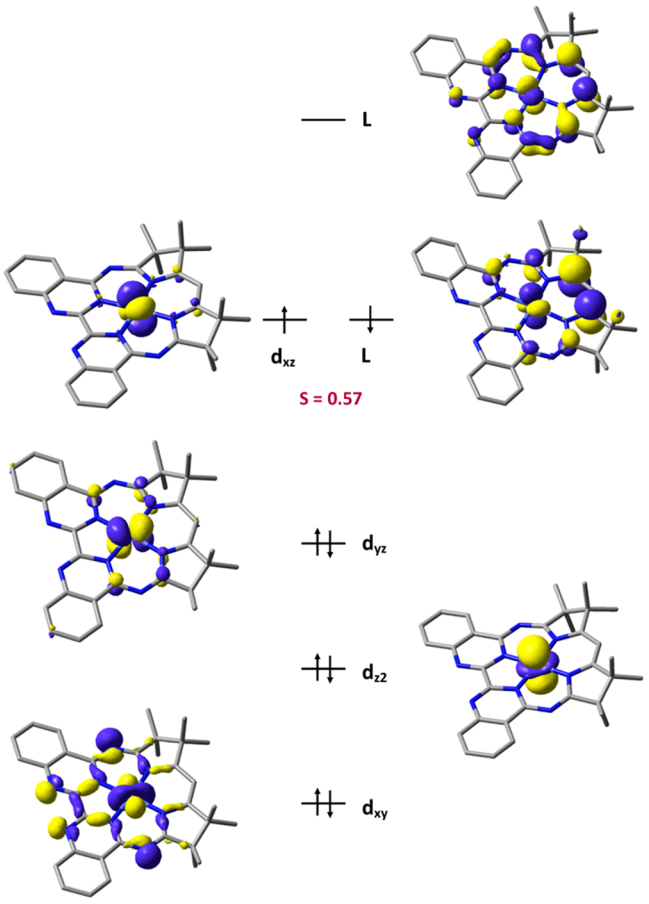

Figure 8. DFT-derived (B3LYP) qualitative molecular orbital diagram of **4** [BS(1,1) calculation on the geometry-optimized structure].

their activity with respect to H_2 production. The Co^I forms of cobaloximes, analogous to vitamin B12, are strong nucleophiles that also readily react with alkylating agents and olefins.

The exact electronic structure of our {Co(Mabiq)} cannot be unambiguously defined owing to the pervasive metal−ligand covalency that precludes assignment of the oxidation states.[22,79] Nevertheless, the combined spectroscopic and DFT data for **4** suggest that significant electron density resides on the diketiminate moiety of the N_4 ligand, such that its true electronic structure lies between the Co^I(Mabiq) and Co^{II}(Mabiq$^\bullet$) limiting forms.

Electrochemistry data illustrate that further reduction of both the Fe(Mabiq) and Co(Mabiq) compounds is possible, yielding the formally "Fe^0" and "Co^0" monoanionic species, respectively. Both of these species are likely to comprise the reduced form of the macrocycle. The Mabiq ligand clearly offers an additional electron storage site, and the redox properties of this ligand render metal-Mabiq compounds promising candidates as catalysts for multielectron reactions. Access to both the one- and two-electron reduced forms of **2** also presents an opportunity to compare the reactivity of both forms with respect to H_2 production. These aspects are the focus of ongoing studies in our group.

A surprising result of our studies was the synthesis of the bimetallic **3**. While the functionalities of Mabiq appear well-suited to the coordination of two metal ions, binuclear compounds had thus far been elusive. We conclude, based on the solution-state spectroscopic data for the binuclear compound, that the second metal site is only weakly bound and readily ousted from the bipyrimidine by competing ligands (e.g., solvent molecules). Nevertheless, the evidence in support of formation of the dicobalt complex in the solid state warrants further examination of the factors that contribute to activation of the second binding site. The coordination chemistry of other metals at this site and modifications to enhance the chelating ability of the external unit are additional research avenues that we are currently exploring.

■ ASSOCIATED CONTENT

Supporting Information

Crystallographic data files (CIF format) and additional electrochemical and spectroscopic data. The Supporting Information is available free of charge on the ACS Publications website at DOI: 10.1021/acs.inorgchem.5b00636.

■ AUTHOR INFORMATION

Corresponding Author

*E-mail: corinna.hess@ch.tum.de.

Present Address

§P.B.: Surface Engineering & Tribology Group, CSIR-Central Mechanical Engineering Research Institute, Mahatma Gandhi Avenue, Durgapur 713209, India.

Notes

The authors declare no competing financial interest.

■ ACKNOWLEDGMENTS

We are grateful to Andreas Göbels (MPI) for technical assistance with SQUID measurements and to Andy Beeby (Durham) for the use of his instrument for diffuse-reflectance spectra. We thank the Diamond Light Source for an award of instrument time on the Station I19 (MT 6749) and the instrument scientists for support. M.K. thanks the TUM Graduate School for financial support. E.V.P. was funded by an EPSRC studentship.

■ REFERENCES

(1) Dempsey, J. L.; Brunschwig, B. S.; Winkler, J. R.; Gray, H. B. *Acc. Chem. Res.* **2009**, *42*, 1995−2004.
(2) Artero, V.; Fontecave, M. *Coord. Chem. Rev.* **2005**, *249*, 1518−1535.
(3) Mahammed, A.; Mondal, B.; Rana, A.; Dey, A.; Gross, Z. *Chem. Commun.* **2014**, *50*, 2725−2727.
(4) Lei, H.; Han, A.; Li, F.; Zhang, M.; Han, Y.; Du, P.; Lai, W.; Cao, R. *Phys. Chem. Chem. Phys.* **2014**, *16*, 1883−1893.
(5) Lee, C. H.; Dogutan, D. K.; Nocera, D. G. *J. Am. Chem. Soc.* **2011**, *133*, 8775−8777.
(6) Jacques, P.-A.; Artero, V.; Pécaut, J.; Fontecave, M. *Proc. Natl. Acad. Sci. U.S.A.* **2009**, *106*, 20627−20632.
(7) Hu, X.; Brunschwig, B. S.; Peters, J. C. *J. Am. Chem. Soc.* **2007**, *129*, 8988−8998.
(8) Du, P.; Schneider, J.; Luo, G.; Brennessel, W. W.; Eisenberg, R. *Inorg. Chem.* **2009**, *48*, 4952−4962.
(9) Dempsey, J. L.; Winkler, J. R.; Gray, H. B. *J. Am. Chem. Soc.* **2010**, *132*, 16774−16776.
(10) Fihri, A.; Artero, V.; Razavet, M.; Baffert, C.; Leibl, W.; Fontecave, M. *Angew. Chem., Int. Ed.* **2008**, *47*, 564−567.
(11) Artero, V.; Chavarot-Kerlidou, M.; Fontecave, M. *Angew. Chem., Int. Ed.* **2011**, *50*, 7238−7266.
(12) Artero, V.; Fontecave, M. *Chem. Soc. Rev.* **2013**, *42*, 2338−2356.
(13) Teets, T. S.; Nocera, D. G. *Chem. Commun.* **2011**, *47*, 9268−9274.
(14) Dempsey, J. L.; Winkler, J. R.; Gray, H. B. *J. Am. Chem. Soc.* **2010**, *132*, 1060−1065.

DOI: 10.1021/acs.inorgchem.5b00636
Inorg. Chem. 2015, 54, 5864−5873

(15) Bhattacharjee, A.; Chavarot-Kerlidou, M.; Andreiadis, E. S.; Fontecave, M.; Field, M. J.; Artero, V. *Inorg. Chem.* **2012**, *51*, 7087−7093.
(16) Roubelakis, M. M.; Bediako, D. K.; Dogutan, D. K.; Nocera, D. G. *Energy Environ. Sci.* **2012**, *5*, 7737−7740.
(17) Solis, B. H.; Hammes-Schiffer, S. *Inorg. Chem.* **2014**, *53*, 6427−6443.
(18) Kellett, R. M.; Spiro, T. G. *Inorg. Chem.* **1985**, *24*, 2373−2377.
(19) Palmer, J. H.; Mahammed, A.; Lancaster, K. M.; Gross, Z.; Gray, H. B. *Inorg. Chem.* **2009**, *48*, 9309−9315.
(20) Solis, B. H.; Maher, A. G.; Honda, T.; Powers, D. C.; Nocera, D. G.; Hammes-Schiffer, S. *ACS Catal.* **2014**, *4*, 4516−4526.
(21) Muresan, N.; Lu, C. C.; Ghosh, M.; Peters, J. C.; Abe, M.; Henling, L. M.; Weyhermüller, T.; Bill, E.; Wieghardt, K. *Inorg. Chem.* **2008**, *47*, 4579−4590.
(22) Lu, C. C.; Bill, E.; Weyhermuller, T.; Bothe, E.; Wieghardt, K. *J. Am. Chem. Soc.* **2008**, *130*, 3181−3197.
(23) Hess, C. R.; Weyhermüller, T.; Bill, E.; Wieghardt, T. *Inorg. Chem.* **2010**, *49*, 5686−5700.
(24) Dzik, W. I.; Xu, X.; Zhang, X. P.; Reek, J. N. H.; de Bruin, B. *J. Am. Chem. Soc.* **2010**, *132*, 10891−10902.
(25) Intrieri, D.; Caselli, A.; Gallo, E. *Eur. J. Inorg. Chem.* **2011**, 5071−5081.
(26) Cui, X.; Xu, X.; Jin, L.-M.; Wojtas, L.; Zhang, X. P. *Chem. Sci.* **2015**, *6*, 1219−1224.
(27) Jin, L.-M.; Lu, H.; Cui, Y.; Lizardi, C.; Arzua, T. N.; Wojtas, L.; Cui, X.; Zhang, X. P. *Chem. Sci.* **2014**, *5*, 2422−2427.
(28) Goswami, M.; Lyaskovskyy, V.; Domingos, S. R.; Buma, W. J.; Woutersen, S.; Troeppner, O.; Ivanović-Burmazović, I.; Lu, H.; Cui, X.; Zhang, X. P.; Reijerse, E. J.; DeBeer, S.; van Schooneveld, M. M.; Pfaff, F. F.; Ray, K.; De Bruin, B. *J. Am. Chem. Soc.* **2015**, *137*, 5468−5479.
(29) Lyaskovskyy, V.; Suarez, A. I. O.; Lu, H.; Jiang, H.; Zhang, X. P.; de Bruin, B. *J. Am. Chem. Soc.* **2011**, *133*, 12264−12273.
(30) Müller, E.; Bernardinelli, G.; von Zelewsky, A. *Inorg. Chem.* **1988**, *27*, 4645−4651.
(31) Banerjee, P.; Company, A.; Weyhermüller, T.; Bill, E.; Hess, C. R. *Inorg. Chem.* **2009**, *48*, 2944−2955.
(32) Hanson, G. R.; Gates, K. E.; Noble, C. J.; Griffin, M.; Mitchell, A.; Benson, S. *J. Inorg. Biochem.* **2004**, *98*, 903−916.
(33) Dolomanov, O. V.; Bourhis, L. J.; Gildea, R. J.; Howard, J. A. K.; Puschmann, H. *J. Appl. Crystallogr.* **2009**, *42*, 339−341.
(34) Sheldrick, G. M. *Acta Crystallogr.* **2008**, *A64*, 112−122.
(35) Neese, F. *ORCA—an ab initio, DFT and semiempirical SCF-MO package*, version 2.9.1; Max Planck Insitut für Bioanorganische Chemie: Mülheim an der Ruhr, Germany, 2009.
(36) Becke, A. D. *J. Chem. Phys.* **1986**, *84*, 4524−4529.
(37) Becke, A. D. *J. Chem. Phys.* **1993**, *98*, 5648−5652.
(38) Lee, C. T.; Yang, W. T.; Parr, R. G. *Phys. Rev. B* **1988**, *37*, 785−789.
(39) Ahlrichs, R.; May, K. *Phys. Chem. Chem. Phys.* **2000**, *2*, 943−945.
(40) Weigend, F.; Ahlrichs, R. *Phys. Chem. Chem. Phys.* **2005**, *7*, 3297−3305.
(41) Schäfer, A.; Huber, C.; Ahlrichs, R. *J. Chem. Phys.* **1994**, *100*, 5829−5835.
(42) Schäfer, A.; Horn, H.; Ahlrichs, R. *J. Chem. Phys.* **1992**, *97*, 2571−2577.
(43) Eichkorn, K.; Treutler, O.; Öhm, H.; Häser, M.; Ahlrichs, R. *Chem. Phys. Lett.* **1995**, *242*, 652−660.
(44) Eichkorn, K.; Weigend, F.; Treutler, O.; Ahlrichs, R. *Chem. Phys. Lett.* **1995**, *240*, 283−290.
(45) Ginsberg, A. P. *J. Am. Chem. Soc.* **1980**, *102*, 111−117.
(46) Noodleman, L.; Peng, C. Y.; Case, D. A.; Mouesca, J. M. *Coord. Chem. Rev.* **1995**, *144*, 199−244.
(47) Kirchner, B.; Wennmohs, F.; Ye, S.; Neese, F. *Curr. Opin. Chem. Biol.* **2007**, *11*, 134−141.
(48) Neese, F. *J. Phys. Chem. Solids* **2004**, *65*, 781−785.
(49) *GaussView 4.1.2*; Gaussian, Inc.: Wallington, CT, 2006.
(50) Liptak, M. D.; Brunold, T. C. *J. Am. Chem. Soc.* **2006**, *128*, 9144−9156.
(51) Bhattarcharjee, A.; Chavarot-Kerlidou, M.; Dempsey, J. L.; Gray, H. B.; Fujita, E.; Muckerman, J. T.; Fontecave, M.; Artero, V.; Arantes, G. M.; Field, M. J. *ChemPhysChem* **2014**, *15*, 2951−2958.
(52) The peak-to-peak separation for all three redox processes in the CV of **4** is 125−150 mV; however, the peak-to-peak separation for the $Fc^{+/0}$ couple was also determined to be 134 mV in THF. Values for i_a/i_c = 0.9−1.
(53) Gavrilova, A. L.; Bosnich, B. *Inorg. Chim. Acta* **2003**, *352*, 24−30.
(54) La Mar, G. N.; Walker, F. A. *J. Am. Chem. Soc.* **1973**, *95*, 1790−1796.
(55) McGarvey, B. M. *Can. J. Chem.* **1975**, *53*, 2498−2511.
(56) Assour, J. M. *J. Am. Chem. Soc.* **1965**, *87*, 4701−4706.
(57) Baumgarten, M.; Winscom, C. J.; Lubitz, W. *Appl. Magn. Reson.* **2001**, *20*, 35−70.
(58) Cariati, F.; Galizzioli, D.; Morazzoni, F.; Busetto, C. *J. Chem. Soc., Dalton Trans.* **1975**, 556−561.
(59) Ozarowski, A.; Lee, H. M.; Balch, A. L. *J. Am. Chem. Soc.* **2003**, *125*, 12606−12614.
(60) Walker, F. A. *J. Am. Chem. Soc.* **1970**, *92*, 4235−4244.
(61) Walker, F. A. *J. Magn. Reson.* **1974**, *15*, 201−218.
(62) Wayland, B. B.; Abd-Elmageed, M. E. *J. Am. Chem. Soc.* **1974**, *96*, 4809−4814.
(63) Hamilton, J. A.; Yamada, R.; Blakley, R. L.; Hogenkamp, H. P. C.; Looney, F. D.; Winfield, M. E. *Biochemistry* **1971**, *10*, 347−355.
(64) Jörin, E.; Schweiger, A.; Günthard, H. H. *J. Am. Chem. Soc.* **1983**, *105*, 4277−4286.
(65) Adamian, V. A.; D'Souza, F.; Licoccia, S.; Di Vona, M. L.; Tassoni, E.; Paolesse, R.; Boschi, T.; Kadish, K. M. *Inorg. Chem.* **1995**, *34*, 532−540.
(66) Hush, N. S.; Woolsey, I. S. *J. Chem. Soc., Dalton Trans.* **1974**, 24−34.
(67) Murakami, Y.; Matsuda, Y.; Sakata, K.; Yamada, S.; Tanaka, Y.; Aoyama, Y. *Bull. Chem. Soc. Jpn.* **1981**, *54*, 163−169.
(68) Ramdhanie, B.; Telser, J.; Caneschi, A.; Zakharov, L. N.; Rheingold, A. L.; Goldberg, D. P. *J. Am. Chem. Soc.* **2004**, *126*, 2515−2525.
(69) Pezeshk, A. *Inorg. Chem.* **1992**, *31*, 2282−2284.
(70) Pzeshk, A.; Greenway, F. T.; Dabrowiak, J. C.; Vincow, G. *Inorg. Chem.* **1978**, *17*, 1717−1725.
(71) Abusamleh, A. S.; Chmielewski, P. J.; Warburton, P. R.; Morales, L.; Stephenson, N. A.; Busch, D. A. *J. Coord. Chem.* **1991**, *23*, 91−111.
(72) Endicott, J. F.; Lilie, J.; Kuszaj, J. M.; Ramaswamy, B. S.; Schmonsees, W. G.; Simic, M. G.; Glick, M. D.; Rillema, D. P. *J. Am. Chem. Soc.* **1977**, *99*, 429−439.
(73) Boča, R.; Miklovič, J.; Titiš, J. *Inorg. Chem.* **2014**, *53*, 2367−2369.
(74) Idešicová, M.; Titiš, J.; Krzystek, J.; Boča, R. *Inorg. Chem.* **2013**, *52*, 9409−9417.
(75) Saber, M. R.; Dunbar, K. R. *Chem. Commun.* **2014**, *50*, 12266−12269.
(76) Titiš, J.; Miklovič, J.; Boča, R. *Inorg. Chem. Commun.* **2013**, *35*, 72−75.
(77) Yang, F.; Zhou, Q.; Zhang, Y.; Zeng, G.; Li, G.; Shi, Z.; Wang, B.; Feng, S. *Chem. Commun.* **2013**, *49*, 5289−5291.
(78) Rosa, V.; Gonzalez, P. J.; Avilés, T.; Gomes, P. T.; Welter, R.; Rizzi, A. C.; Passeggi, M. C. G.; Brondino, C. D. *Eur. J. Inorg. Chem.* **2006**, 4761−4769.
(79) Sproules, S.; Kapre, R. R.; Roy, N.; Weyhermüller, T.; Wieghardt, K. *Inorg. Chim. Acta* **2010**, *363*, 2702−2714.

DOI: 10.1021/acs.inorgchem.5b00636
Inorg. Chem. 2015, 54, 5864−5873